

An electrofusion chip with a cell delivery system driven by surface tension

Jongil Ju¹, Jung-Moon Ko^{2,3}, Hyeon-Cheol Cha², Joong Yull Park¹,
Chang-Hwan Im⁴ and Sang-Hoon Lee¹

¹ Department of Biomedical Engineering, College of Health Sciences, Korea University, Jeongneung 3(sam)-dong, Seongbuk-gu, Seoul 136-703, Korea

² Department of Biology, Dankook University, Anseo-dong, Cheonan 330-714, Korea

³ NAVIBIOTECH #208 BI Center, San 29, Anseo-dong, Cheonan 330-714, Korea

⁴ Department of Biomedical Engineering, Yonsei University, 234 Maeji-ri, Heungeop-myun, Wonju 220-710, Korea

E-mail: dbiomed@korea.ac.kr (Sang-Hoon Lee)


Received 18 July 2008, in final form 20 October 2008


Published 27 November 2008

Online at stacks.iop.org/JMM/19/015004

Abstract

We have fabricated an electric cell fusion chip with an embedded cell delivery function driven by surface tension and evaluated its performance with several types of plant cells. The chip consists of a polydimethylsiloxane-based microchannel with a fusion chamber and gold–titanium (Au–Ti) electrodes. The velocity profiles of the microfluid in the channel and fusion chamber were calculated to predict cell movement, and the electric field distribution between the electrodes was also calculated in order to determine the appropriate electrode shape. The range of the fluid velocity in the fusion chamber is 20–50 $\mu\text{m s}^{-1}$ and the measured speed of the cells is approximately 45 $\mu\text{m s}^{-1}$, which is sufficiently slow for the motion of the cells in the fusion chamber to be monitored and controlled. We measured the variation of the pearl chain ratio with frequency for five kinds of plant cells, and determined that the optimal frequency for pearl chain formation is 1.5 MHz. The electrofusion of cells was successfully carried out under ac field (amplitude: 0.4–0.5 kV cm^{-1} , frequency: 1.5 MHz) and dc pulse (amplitude: 1.0 kV cm^{-1} , duration: 20 ms) conditions.

 This article features online multimedia enhancements

 This article has associated online supplementary data files

(Some figures in this article are in colour only in the electronic version)

1. Introduction

Cell fusion is an important cellular process that occurs during the differentiation of muscle and bone cells, during embryogenesis and during morphogenesis. Therefore, the fusion under the *in vitro* environment is important in understanding cell properties. The electrofusion of cells is an important achievement of modern biology and biotechnology, with applications including the engineering of hybridoma for antibody production, cloning of mammals, determining the genetic make-up of organisms, and vaccination against cancer [1–4] and production of new species [5, 6]. Fusion of plant protoplasts with protoplasts from different species

can provide an ideal system for genetic modification and for use in plant breeding. Electrofusion will minimally yield comparable results to chemical fusions, at least in systems with robust protoplasts in good chemical fusion protocols [5], and will do better with fragile protoplasts [6]. In addition, the most valuable aspects of electrofusion techniques are the high fusion frequencies attained, often tenfold higher than analogous chemical systems [7]. The concept of cell–cell electrofusion was first reported by Senda *et al* [8] in 1979, and pioneering research in electrofusion was carried out by Zimmermann and his co-workers [9, 10], who demonstrated the electrofusion of plant protoplasts from *Vicia faba* mesophyll cells in large numbers in a 1 mL fusion

chamber with parallel electrodes. Morikawa *et al* electrofused mesophyll protoplasts from *N. glauca* and *N. langsdorffii* and obtained colonies that when cultured grew vigorously for 10 weeks [11]. The electrofusion technique overcomes the limitations of conventional chemically or virally induced cell fusion such as cell toxicity, long fusion periods [12] and the complexity of the fusion process.

However, most conventional electrofusion has been performed with a large number of cells, because the control of the fusion process at the level of a few cells is difficult in systems that are not fabricated with microtechnology. The need to manipulate a single cell or a few cells has recently increased, so a few electrofusion chips that use micro electro mechanical system (MEMS) technology have been developed [4, 13–16]. Although the concept of MEMS technology is attractive, practical electrofusion processes are complicated because they require a fluidic channel with a high aspect electrode created by metal deposition, patterning and electroplating, and complicated peripheral devices such as syringe or peristaltic pumps. In particular, these devices need high-precision delivery systems that transport the cells at a speed sufficiently slow for the cells' movements to be monitored.

In this paper, we report the fabrication of a polydimethylsiloxane-based electrofusion chip with an embedded cell-delivery function. Its slow-pumping mechanism uses a micropump that drives flow in the microchannel by using only the surface tension of the inlet and outlet droplets [17, 18]. One feature of our fusion chip is that its fabrication is very simple and cost effective (the fabrication time is less than 1 day once the master mold has been prepared). The embedded delivery system is another important feature of this chip, which means that complicated peripherals are not required. The slow delivery of cells usually requires a precise and expensive pump, and even then dead volume is a common problem. The embedded surface tension passive pump addresses these issues. Further, the pressure required to deliver cell suspension media is small, which means that the process combining polydimethylsiloxane (PDMS) and the electrode is very simple. The electric field distribution and the flow velocity in the fusion chamber were calculated using 3D finite element method (FEM) software and computational fluid dynamics (CFD) code. The cell delivery and fusion processes of this chip were tested, and we measured the variation of pearl chain formation [19, 20] with the frequency of the ac field to determine the optimal frequency for the cells of five different plants (*Arabidopsis thaliana*, *Nicotiana tabacum*, *Peucedanum japonicum*, *Glehnia littoralis* and *Brassica campestris*).

2. Materials and methods

2.1. Preparation of the protoplasts

To isolate the protoplasts, we used the modified Sun's method [21, 22]. Fully expanded leaves of the samples (*Brassica campestris*, *Arabidopsis thaliana*, *Nicotiana tabacum*, *Peucedanum japonicum* and *Glehnia littoralis*) were

surface-sterilized with 2% sodium hypochlorite for 10 min and then washed four times with distilled water. The lower epidermal layers of the leaves were carefully removed with sharp-tipped forceps or cut into small pieces. The leaf pieces were carefully placed onto the surface of an enzyme solution (2.0% [w/v] cellulase Onozuka R-10, 0.5% [w/v] macerozyme, 0.1% [w/v] hemicellulase in the Cell and Protoplast Washing salt solution (CPW) 13 M, pH 5.8) with the lower surface facing down and incubated at 25 °C for 12 h to release the protoplasts. The digested leaf pieces were filtered through a steel mesh (40 by 100 in; Sigma, St Louis, MO, USA), and the enzyme mixture was centrifuged at 600 rpm for 10 min. The upper part of the enzyme mixture was discarded, and then the protoplasts were resuspended and washed twice with a washing solution (CPW 13M) by using centrifugation and resuspension. To extract healthy protoplasts, the protoplast suspension was floated on a CPW 21S solution (21% [w/v] sucrose in CPW solution, pH 5.8) and centrifuged at 600 rpm for 15 min. Protoplasts in the upper layer of the CPW 21S solution were pipetted and washed with a hypertonic fusion solution (0.5 M mannitol and 1 mM CaCl₂), and the density of the protoplast suspension was adjusted to $1 \times 10^5 \text{ mL}^{-1}$.

2.2. Fabrication of the electrofusion system

The electrofusion chip has two components: the microchannel containing the fusion chamber, the inlet–outlet ports and the cell delivery channel, and the microelectrodes, which provide the electrical power for electrofusion. 3D schematic diagrams of the PDMS-based microfluidic chip and its dimensions are shown in figures 1(a) and (b) and the photograph of the electrofusion chip with electrodes is shown in figure 1(c). The microchannels were fabricated with PDMS (Sylgard 184, Dow Corning, USA) by using a previously reported procedure [23], and the microelectrodes were created by carrying out e-beam evaporation of titanium and gold onto the glass slide and chemical patterning [24]. The thickness of the microchannel for the delivery of the cells and the media is 100 μm , and the thickness of the fusion chamber and the inlet-outlet ports is 600 μm . The processes of fabrication of the microchannels and microelectrodes are illustrated in supplementary information S1 and S2 respectively (available at stacks.iop.org/JMM/19/015004). We now provide a brief description of the electrode construction process and the integration of the electrode and the PDMS-based microchannel: (1) the titanium (the seed layer, thickness: 200 Å) and gold (the electrode layer, thickness: 2000 Å) layers are deposited onto the glass slide by using e-beam evaporation. (2) The microelectrode patterns are created via photoresist masking and chemical etching (Au etchant: aqua regia (HNO₃ + 3HCl), Ti etchant: (HF + 2HNO₃ + 7H₂O)). (3) The PDMS microchannel is placed on the electrode-patterned glass slide and pressed lightly with a finger. The volume of the fusion chamber is 0.825 mm³. An openable PDMS cover was placed into the top of the fusion chamber to enable the removal of the fused cells with a micropipette [25].

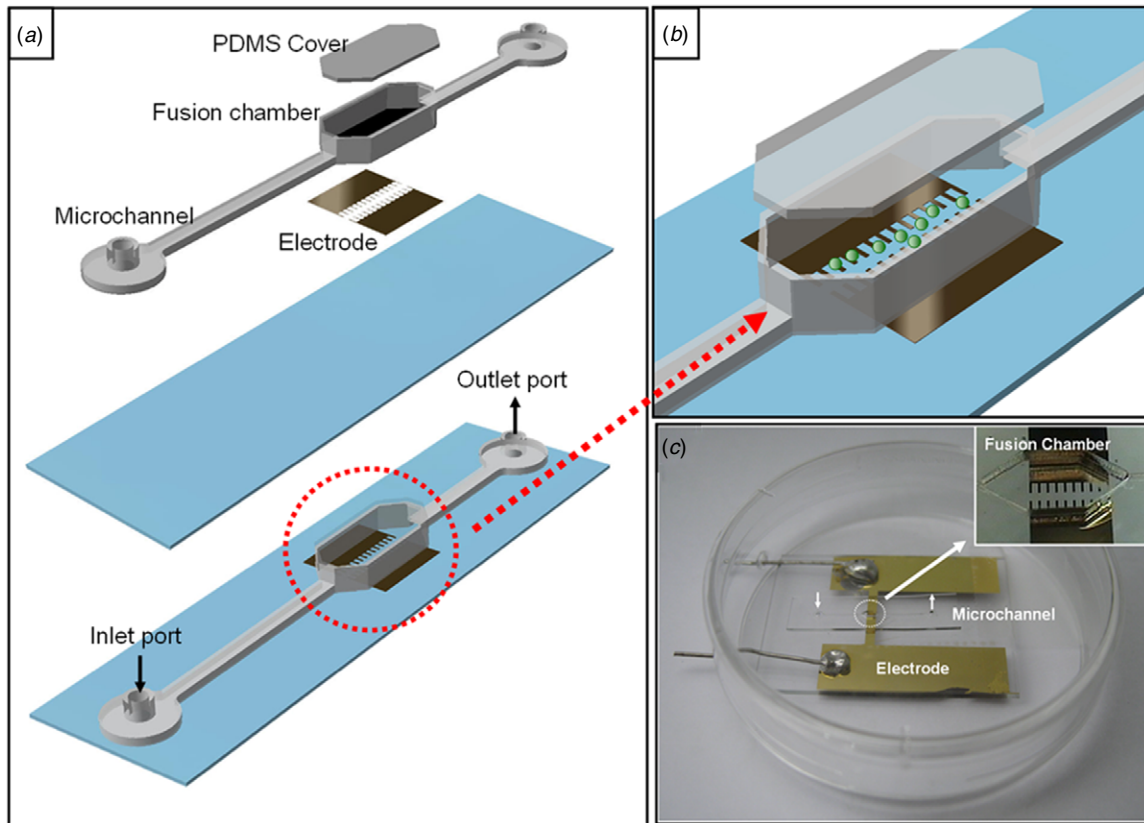


Figure 1. Schematic diagrams of the 3D electrofusion chip: (a) the elements of the electrofusion chip and the assembled electrofusion chip (dimensions: microchannel (H : 0.2 mm, W : 0.1 mm, L : 17 mm), fusion chamber (H : 0.6 mm, W : 0.6 mm, L : 2 mm), inlet port and outlet port (H : 0.6 mm, D : 0.7 mm), H : height, W : width, L : length, D : diameter); (b) the region of cell fusion and the electrode. (c) A photograph of the electrofusion chip. Inset photograph of the electrofusion chamber with electrodes.

2.3. Numerical analysis of the flow inside the channel

To locate the cells in suitable positions in the fusion chamber, an understanding of the flow velocity in the cell delivery channel and the fusion chamber is important. We calculated the velocity profile in the electrofusion chip. It is well known that the following Young–Laplace equation explains the generation of flow by surface tension [17, 18]:

$$\Delta P_{\text{static}} = \Delta P_i - \Delta P_o = 2\gamma \left(\frac{1}{r_i} - \frac{1}{r_o} \right) \quad (1)$$

where P is the pressure, ΔP is the pressure difference, γ is the surface tension coefficient, r is the radius of a droplet and the subscripts static, i and o denote the static state, the inlet port and the outlet port, respectively.

Under the assumption of static inlet and outlet pressure (the initial pressure), the finite volume method (FVM) was applied using the commercially available software GAMBIT 1.2 (Fluent, USA) and FLUENT 5.5 (Fluent, USA). A structured grid system was used for most of the regions of the chip. The total grid number was approximately 90 000. The fluid was assumed to be water (a homogeneous, incompressible Newtonian fluid with a density of 998.2 kg m^{-3} and a dynamic viscosity of $0.001 \text{ kg m}^{-1} \text{ s}^{-1}$) with a laminar and steady flow, as is reasonable for the low Reynolds number flows in microfluidic systems. The Navier–Stokes flow motion equations and the conservation equation were

solved. Pressure boundary conditions were set at the inlet (10, 20, 30, 40 and 50 Pa) and the outlet (0 Pa). Convergence was regarded as achieved when the residuals of the momentum and conservation equations reached 10^{-6} .

2.4. Numerical analysis of the electric field between the electrodes

The cells in the fusion chamber are relocated between the electrodes by the application of ac (alternating current) fields, so the electrophoretic force plays a key role. Thus, an understanding of the electric field distributions for the relevant electrodes is important to the prediction of the behavior of the cells within the electric field. We investigated the electric field for electrodes with two different thicknesses (thin and thick) and for two adjacent electrodes with two different pitches (a narrow gap and a wide gap).

The electric field distribution between the two electrodes was analyzed with the 3D finite element method (FEM). Since the electrical conductivity of the medium is sufficiently small to be neglected, a simple Laplace equation describing the electrostatic field was used as the governing equation of the analysis. We used a first-order finite element formulation and the ICCG matrix solver [26]. The analysis models were designed and tessellated into tetrahedral elements by using the freeware TetGen version 1.4.2 (downloadable at <http://tetgen.berlios.de>). The electrode pair was analyzed

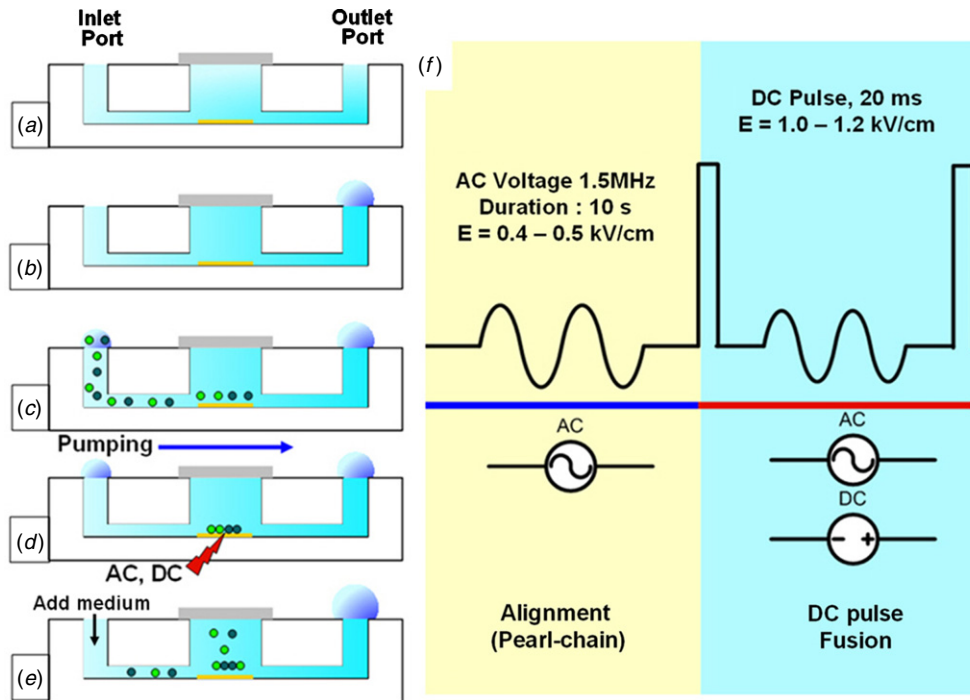


Figure 2. Schematic diagrams of the cell delivery and fusion processes: (a) a microchannel filled with a hypertonic fusion solution; (b) the dropping of a hypertonic fusion solution into the outlet port; (c) the dropping of mixed protoplasts into the inlet port; (d) the application of an ac field and a dc pulse for the alignment and electrofusion of the protoplasts; (e) hypertonic fusion solution exchange of the culture media and a fused cell culture; (f) properties of the ac field and the dc pulse for the electrofusion of the protoplasts.

with periodic boundary conditions because of the heavy computational burden of the 3D analysis. In the analysis of the electrodes with different thicknesses, 42 434 nodes and 234 558 tetrahedral elements were generated for the thin electrode (wide gap) and 36 950 nodes and 201 322 elements were generated for the thick electrode. For the narrow gap, 59 922 nodes and 341 310 elements were generated. Fixed boundary conditions were imposed at both electrodes: 1 V at the upper electrode and -1 V at the lower electrode. Since the electrical permittivity of the homogeneous medium does not affect the electric field intensity, the relative permittivity (ϵ_r) was assumed to be 1. The simulations were carried out with a PC (CPU: Pentium IV 3.4 GHz; Memory: 2 GB).

2.5. Cell delivery and electrofusion experiments

The delivery of cells is achieved in this chip by using surface tension passive pumping. Figure 2 shows schematic diagrams of the passive pumping and electrofusion processes, and the details are as follows. The microchannel is filled with a hypertonic fusion solution by using a micropipette (figure 2(a)). The hypertonic fusion solution (about $30 \mu\text{L}$) is dropped into the outlet port as shown in figure 2(b) and the mixture of protoplasts and hypertonic solution (about $10 \mu\text{L}$) is dropped into the inlet port (figure 2(c)); then the mixed protoplasts slowly flow into the microchannel due to the difference between the surface tensions of the inlet and outlet droplets. The flow is very slow in the fusion chamber, so the operator can monitor the movement of cells with the microscope. An ac field (amplitude: $0.4\text{--}0.5 \text{ kV cm}^{-1}$;

frequency: 1.5 MHz) with rectangular waveform is applied to the microelectrodes, which results in the formation of pearl chains between the electrodes (figure 2(d)), and a short and high voltage dc pulse (amplitude: $1.0\text{--}1.2 \text{ kV cm}^{-1}$; duration: 20 ms) is applied to produce the fusion of cells when the cells are in close contact with each other due to the dielectrophoretic force. Figure 2(f) shows a sequence of the electric waveform in detail. Finally, the culture medium (Nitsch medium supplemented with growth regulators [27]) is dropped into the inlet port (figure 2(e)) to replace the hypertonic fusion solution.

3. Results and discussion

3.1. Fabrication of the fusion chip

The photograph of the fabricated fusion chip is shown in figure 1(c) and this chip functioned well as we intended. In our fusion chip, the PDMS channel is adhered on the electrode-patterned glass slide only by slight pressing with a finger without the plasma bonding process, which indicates that a PDMS channel is adhered only by the stickiness of PDMS. Despite such weak adhesion, the cell suspension medium driven by an incorporated passive pumping system passed through the channel without any leakage. Usually, the complete bonding of an electrode patterned glass and a PDMS channel requires a complicated and time consuming process. But, our fusion chip including a passive pump addressed lots of difficulties in the bonding process. In addition, the glass slide and the PDMS channel can be separated manually

once the measurements have been completed, which indicates that the PDMS channels are disposable, and each electrode-patterned glass slide is reusable after cleaning with ethyl alcohol.

3.2. Velocity field in the microchannel and delivery of cells to the fusion chamber by passive pumping

A CFD-based simulation was carried out to calculate the velocity profiles in the microchannel and fusion chamber, and the results are shown in figure 3. The mean velocity in the microchannel is approximately $40 \mu\text{m s}^{-1}$ when the pressure difference (ΔP) is 30 Pa, and this flow speed is sufficient to transport cells to the fusion chamber. (The simulation was carried out for a height from the bottom of the microchannel of $50 \mu\text{m}$, see figure 3(a).) The mean velocities for ΔP ranging from 10 to 50 Pa with an interval of 10 Pa were calculated and are in good agreement with the experimental mean velocities, as shown in figure 3(e). The experimental mean velocity was measured by using polystyrene (diameter: $20 \mu\text{m}$) beads. The beads were introduced into the channel and their mean speed of flow was determined from a video clip. When ΔP is 30 Pa, the expansion of the cross-sectional area of the fusion chamber means that the velocity decreases to $20\text{--}50 \mu\text{m s}^{-1}$ depending on the distance from the sidewall of the fusion chamber (figure 3(c)), and similar contour patterns were observed for ΔP of 10 and 50 Pa (figures 3(b) and (d) respectively). There are two advantages to this widely spread slow flow in the fusion chamber: (1) the cells are uniformly located in the fusion chamber, and (2) the pearl chains formed between the electrodes are maintained as the flow continues.

The behavior of the cells was observed at a pressure difference of 30 Pa ($10 \mu\text{L}$ (inlet) and $30 \mu\text{L}$ (outlet) droplets were used). The speeds of the cells were found to be similar to the simulation results. The measured mean cell speed was approximately $45 \mu\text{m s}^{-1}$, which is sufficiently slow that the motion of the cells can be monitored with an optical microscope. We also found that the pearl chain formation rate is high when the pressure is in the range $20\text{--}30$ Pa (figure 4(b)) but this rate decreases significantly when the velocity is too high, as shown in figure 4(a) (because the cells move too rapidly past the electrodes), or too slow, as shown in figure 4(c) (because the cells tend to aggregate). During the pumping process, the cells were found to be safely transported, with no rupture of the cell membranes observed in microscopic inspections.

(Video clips of *Peucedanum japonicum* and *Glehnia littoralis* cell transportation are included in the supplementary materials S3 available at stacks.iop.org/JMM/19/015004.)

3.3. Analysis of the electric field between the two electrodes

In a homogeneous medium, the determination of electrode dimensions, interval and shape is important to improve the pearl chain formation and fusion performance. We investigated the effects of varying the electrode thickness (rectangular electrodes, one thin ($0.2 \mu\text{m}$) and one thick ($100 \mu\text{m}$)) on the electric field distribution and of varying

the interval between the electrodes by using a 3D FEM model. First, the electric field distributions around the thin and thick electrodes were calculated for four cross-sectional planes (heights: $0.2 \mu\text{m}$, $20 \mu\text{m}$, $50 \mu\text{m}$ and $100 \mu\text{m}$ from the electrodes). The results are shown in figure 5. The electric field distribution of the thin electrode is shown in figure 5(a) and that of the thick electrode in figure 5(b). The alignment of the cells is crucial to the efficiency of cell fusion, and a uniformly distributed electrical field between the electrodes is an important factor for better alignment [28–31]. The electric field of the thin electrode was found to decrease rapidly as the height of the channel increases, whereas the electric field of the thick electrode is uniform. Therefore, the dielectrophoretic force ($F_{\text{DEP}} = K \cdot \nabla E^2$) between the upper and lower electrodes will decrease as the height of the channel increases in the case of the thin electrode, which indicates that the dragging force aligning the cells will decrease.

The simulation results suggest that the thicker electrode should provide better conditions for cell alignment and fusion. However, our experimental results show that the thin electrode provides an electric field that induces the cells to form pearl chains and undergo electric fusion. The reason for this is that most of the cells move on the surface of electrode patterned glass due to the gravitation under such a slow flow condition (see the supplementary materials, figure S4 and S4-1, available at stacks.iop.org/JMM/19/015004). The thin electrode has many advantages for the easy fabrication of chips, especially when combining a PDMS channel with electrode-patterned glass. We also investigated the effect of varying the pitch between the adjacent electrodes on the electric field. The FEM simulations were carried out by varying the pitch (75 and $100 \mu\text{m}$) and the results are shown in figure 6. As the pitch becomes narrower, the influence of the adjacent electrode increases and the electric fields between the upper and lower electrodes (see the dotted area in figure 5) become almost uniform. However, as the pitch becomes wider, the influence of the adjacent electrodes decreases and the electric fields between confronting upper and lower electrodes are higher than that of the adjacent electrode, so we expect that pearl chain formation will be better for wider pitches. These results show that the determination of the appropriate pitch is important in the design of cell fusion systems.

3.4. Determination of the optimal ac frequency

Pearl chain formation enhances electrofusion performance. We define the pearl chain ratio as the number of pearl chained electrodes/total number of electrodes and measure the variation of the pearl chain ratio with the ac frequency. For the efficient measurement of the pearl chain ratio, an electrode array (25 ea) was fabricated for the mass electrofusion of protoplasts. We measured the pearl chain ratio for various frequencies (0.5 , 1 , 2 , 3 , 5 and 10 MHz; amplitude: $0.4\text{--}0.5 \text{ kV cm}^{-1}$), and this experiment was carried out for five cell types: *Arabidopsis thaliana*, *Nicotiana tabacum*, *Peucedanum japonicum*, *Glehnia littoralis* and *Brassica campestris*, in order to determine a broadly applicable frequency range. Figure 7 shows the variation of the pearl chain ratio with

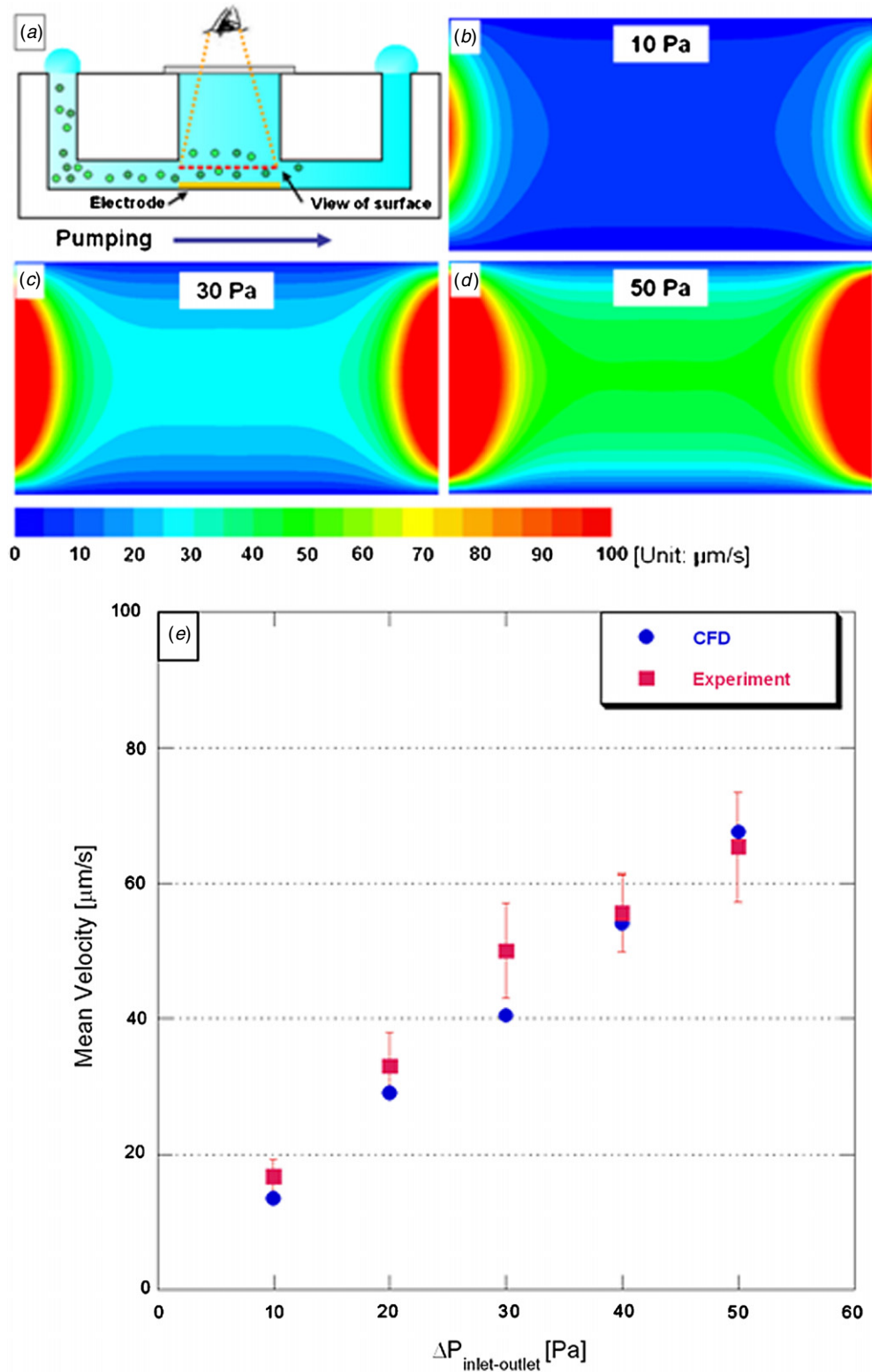


Figure 3. The numerical analysis of the mean velocity field inside the fusion chamber. The simulations were carried out for a surface $50 \mu\text{m}$ above the bottom of the microchannel. (a) Cross-sectional view of the electrofusion chip and the observation surface. (b) The mean velocity field for $\Delta P = 10 \text{ Pa}$. (c) The mean velocity field for $\Delta P = 30 \text{ Pa}$. (d) The mean velocity field for $\Delta P = 50 \text{ Pa}$. (e) The variation of the mean velocity with the differential pressure. The circles are calculated data and the squares are experimental data.

the frequency for each cell type. The pearl chain ratios of all the cells are better in the range 1–2 MHz than in other frequency ranges. This optimal frequency range is similar to that found by other groups [28–30]. We also define the

cell trapping rate as the number of trapped cells/total number of cells. The cell trapping rate was estimated by carrying out cell counting and measurements of the trapping rate, and we found that approx. $92.2 \pm 2.3\%$ of the cells near the

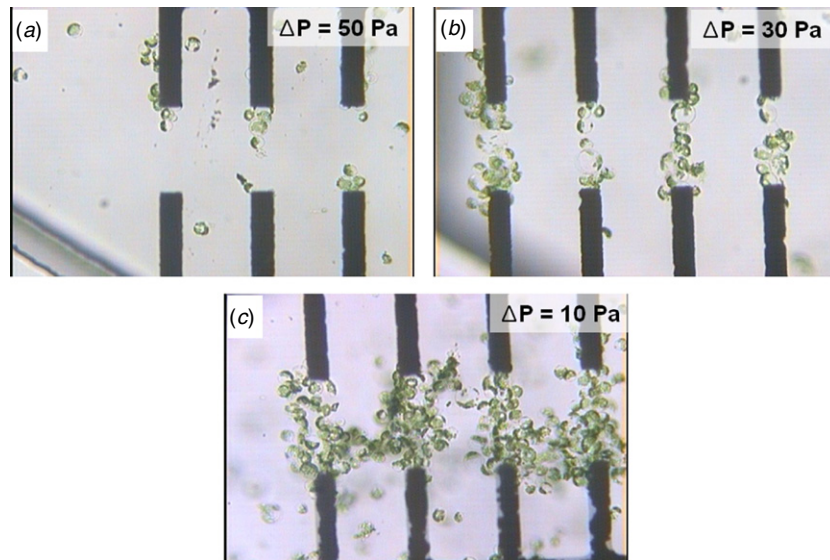


Figure 4. The dependence of the pearl chain formation rate on the differential pressure: (a) the differential pressure is 50 Pa (inlet droplet volume $5 \mu\text{L}$, outlet droplet volume $30 \mu\text{L}$); (b) the differential pressure is 30 Pa (inlet droplet volume $10 \mu\text{L}$, outlet droplet volume $30 \mu\text{L}$); (c) the differential pressure is 10 Pa (inlet droplet volume $20 \mu\text{L}$, outlet droplet volume $60 \mu\text{L}$).

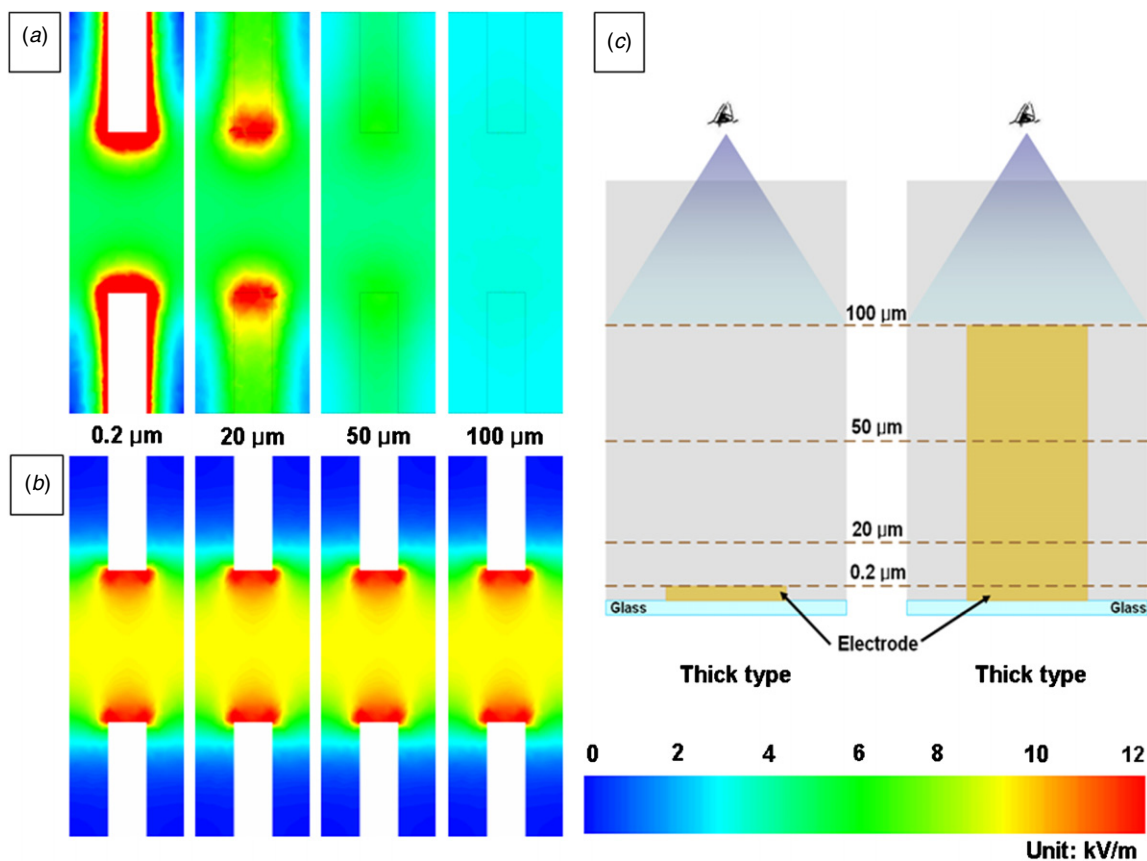


Figure 5. Schematic diagrams of the electric field distributions for electrodes with two different thicknesses: (a) a thin electrode with a thickness of $0.2 \mu\text{m}$; (b) a thick electrode with a thickness of $100 \mu\text{m}$. (c) Schematic diagrams of the cross-sectional views of the thin and thick electrodes, and the observation surface.

surface of the channel are trapped by the electrode when the flow speed is less than $40 \mu\text{m s}^{-1}$. At low flow rates, the cells sink and move on the surface of the electrode due to

gravitation, so most of cells are trapped when the electric field is applied (see the supplementary materials figure S4 and S4-1 available at stacks.iop.org/JMM/19/015004); this is another

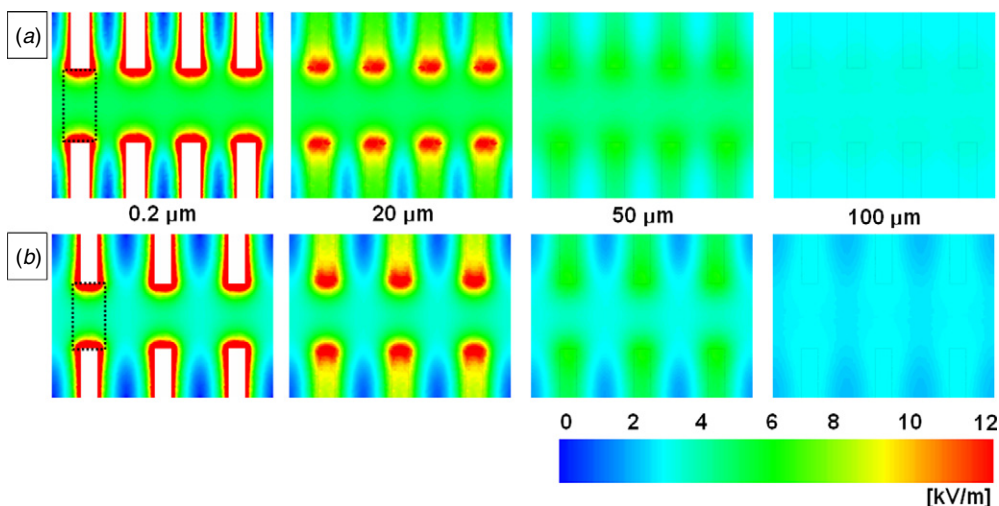


Figure 6. Schematic diagrams of the electric field distribution for adjacent electrodes with two different pitches; the heights of the observation surfaces are 0.2 μm, 20 μm, 50 μm and 100 μm from the bottom of the microchannel: (a) a narrow gap (the pitch between the adjacent electrodes is 75 μm); (b) a wide gap (the pitch between the adjacent electrodes is 100 μm).

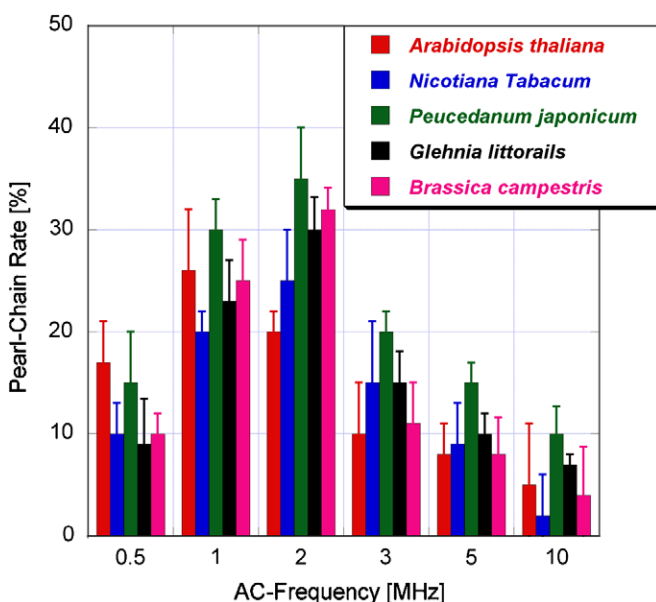


Figure 7. Variations of the pearl chain ratios with the ac frequency of five different plant cells. The five plants are *Arabidopsis thaliana*, *Nicotiana tabacum*, *Peucedanum japonicum*, *Glehnia littoralis* and *Brassica campestris*.

advantage of the integrated surface tension pump. A video clip of cell trapping is available in the supplementary materials S3 available at stacks.iop.org/JMM/19/015004.

3.5. Electrofusion of protoplasts

The cell fusion mechanism is well known. A little pore is generated on the membrane of protoplasts that are in contact, and the two cells fuse resulting in a single cell as a result of surface tension [31]. Figure 8 shows micrographs of the protoplast (*Peucedanum japonicum* and *Glehnia littoralis*) fusion process in the fusion chamber with electrodes separated by a 200 μm gap. Figure 8(a) shows pearl chain formation

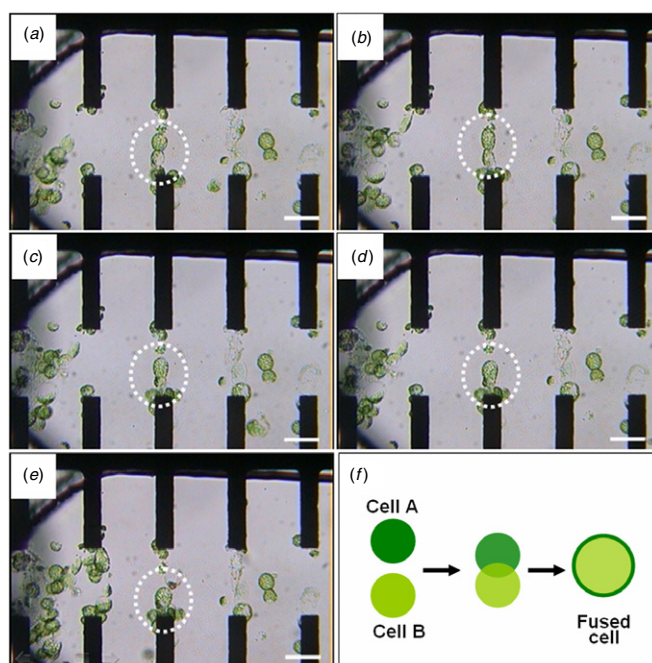


Figure 8. Experimental observations of a protoplast (*Peucedanum japonicum* and *Glehnia littoralis*) fusion system. (a) Pearl chain formation under the ac field (amplitude: 0.4–0.5 kV cm⁻¹; frequency: 1.5 MHz). (b) The fusion is in progress and the contact zone between the protoplasts, which is in the vicinity of the microelectrodes, is no longer distinct. Due to electrotoporation in the hypertonic fusion solution, the protoplasts are somewhat tumid. (c) and (d) The fusion is nearly complete. The grayish line that appears to divide the fused cell into two halves is the waist of the dumbbell shape of the fused cell. Because the cytoskeletons are intact inside the protoplasts, complete rounding of the fused cell has not yet been achieved. (e) A gentle pulling force was applied through the microelectrodes to show that the cells are fused. Scale bar is 100 μm. (f) Schematic diagrams of fusion sequence of two cells.

under an ac field (amplitude: 0.4–0.5 kV cm⁻¹; frequency: 1.5 MHz); the chain between the two electrodes is stable.

Figure 8(b) shows the initiation of the fusing process that arises on membrane breakdown after the application of a dc pulse (amplitude: 1.0 kV cm^{-1} ; duration: 20 ms). Cell fusion then proceeds slowly over 5 min, as shown in figures 8(c) and (d), and the membranes of the two cells become combined. The fused cell is dumbbell shaped at this stage, because the cytoskeletons are still intact inside the protoplasts. After 10 min, the fused cell spontaneously becomes round (figure 8(e)), and the cell culture medium is supplied to the fusion chamber with the surface tension pumping system to provide nutrient to the fused cells. Figure 8(f) shows fusion sequence of two cells. This delivery of the culture medium through passive pumping does not affect the fused cells, which demonstrates the excellent cell and media transport capabilities of the chip. Our microchip-based electrofusion process has several advantages. For example, cells can be kept in a physiological buffer until fusion, and all fusion processes can be carried out under the control of an operator beneath an inverted microscope (Leitz DM-IL, Germany). Thus a fresh post-fusion medium (the culture medium) such as the Nitsch medium for cell recovery [22] can be delivered to the fused cells without resulting in any damage to the fused cells. The possibility of infection is reduced because all the processes are carried out inside the chip.

After the cells have fused, their collection is very important. We created small windows in the chip to retrieve the fused cells using a micropipette under the stereoscope. It is also possible to culture the fused cells inside the fusion chamber just by replacing the medium and then monitoring them. By using the passive pumping system, fresh media can easily be introduced. In this work, we measured the fusion rate under an optimized condition with various plant cell types; the maximum fusion rate was 3–5%.

4. Conclusions

In this study, an electrofusion device with cell and nutrient delivery functions was successfully designed and fabricated, and its performance was evaluated with protoplasts from various species. The cells were transported safely into the fusion chamber and electrofusion was successfully carried out with an ac field and dc pulses. To the best of our knowledge, this electrofusion chip with its passive delivery function is the first of its kind; this chip provides simple and cost-effective cell and nutrient delivery. This electrofusion chip should have many applications in the electrofusion and culture of mammalian, fungal, and plant cells. It should also be useful in applications related to gene transfection.

Acknowledgments

This study was supported by a grant (M103KV010031-07K2201-03110) from brain research center of the 21st century frontier research program and a grant (ROA-2007-000-20086-0) from the Korea Science and Engineering Foundation (KOSEF) through the NRL program funded by the Ministry of Science and Technology, the Republic of Korea.

References

- [1] Voldman J 2006 Electrical forces for microscale cell manipulation *Annu. Rev. Biomed. Eng.* **8** 425–54
- [2] Strömberg A, Ryttsén F, Chiu D T, Davidson M, Eriksson P S, Wilson C F, Orwar O and Zare R N 2000 Manipulating the genetic identity and biochemical surface properties of individual cells with electric-field-induced fusion *Proc. Natl Acad. Sci.* **97** 7–11
- [3] Neumann E, Sowers A E and Jordan C A 1989 *Electroporation and Electrofusion in Cell Biology* (New York: Plenum)
- [4] Tresset G and Tekeuchi S 2004 A microfluidic device for electrofusion of biological vesicles *Biomed. Microdevices* **6** 213–8
- [5] Fish N, Karp A and Jones M G K 1988 Production of somatic hybrids by electrofusion in Solanum *Theor. Appl. Genet.* **76** 260–6
- [6] Negrutiu I, De Brouwer D, Watts J W, Sidorov V I, Dirks R and Jacobs M 1986 Fusion of plant protoplasts: a study using auxotrophic mutants of *Nicotiana plumbaginifolia* Viviani *Theor. Appl. Genet.* **72** 279–86
- [7] Zachrisson A and Bormann C H 1986 Application of electric fields fusion in plant tissue culture *Physiol. Plantarum.* **61** 314–20
- [8] Senda M, Takeda J, Abe S and Nakamura T 1979 Induction of cell fusion of plant protoplasts by electrical stimulation *Plant Cell Physiol.* **20** 1441–3
- [9] Zimmermann U and Scheurich P 1981 High frequency fusion of plant protoplasts by electric fields *Planta* **151** 26–32
- [10] Zimmermann U, Vienken J and Pilwat G 1984 Electrofusion of cells *Investigative Microtechniques in Medicine and Biology* vol 1 ed J Chayen and L Bitensky (New York: Dekker)
- [11] Morikawa H, Sugino K, Hayashi H, Takeda J, Senda M, Hirai A and Yamada Y 1986 Interspecific plant hybridization by electrofusion in *Nicotiana* *Nat. Biotechnol.* **4** 57–60
- [12] Van Wert S L and Saunders J A 1992 Electrofusion and electroporation of plants *Plant Physiol.* **99** 365–7
- [13] Tresset G and Shoji 2005 Utilization of cell-size lipid containers for nanostructure and macromolecule handling in microfabricated device *Anal. Chem.* **77** 2795–801
- [14] Chiu D T 2001 A microfluidics platform for cell fusion *Curr. Opin. Chem. Biol.* **5** 609–12
- [15] Masuda S, Washizu M and Nanba T 1989 Novel method of cell-fusion in field constriction area in fluid integrated-circuit *IEEE Trans. Ind. Appl.* **25** 732–7
- [16] Voldman J, Gray M L, Toner M and Schmidt MA 2002 A microfabrication-based dynamic array cytometer *Anal. Chem.* **74** 3984–90
- [17] Walker G M and Beebe D J 2002 A passive pumping method for microfluidic devices *Lab Chip* **2** 131–4
- [18] Berthier E and Beebe D J 2007 Flow rate analysis of a surface tension driven passive micropump *Lab Chip* **7** 1475–8
- [19] Griffin J L and Ferris C D 1970 Pearl chain formation across radio frequency fields *Nature* **226** 152–4
- [20] Sowers A E 1984 Characterization of electric field-induced fusion in erythrocyte ghost membranes *J. Cell Biol.* **99** 1989–96
- [21] Ko J-M, Ju J, Lee S and Cha H-C 2006 Tobacco protoplast culture in a polydimethylsiloxane-based microfluidic channel *Protoplasma* **227** 237–40
- [22] Sun T-H, Xue Q-Z, Ding C-M, Zhang X-Y, Zhang L-L, Wang W-F and Ali S 2005 Somatic hybridization between *Nicotiana tabacum* and *N. repanda* based on a single inactivation procedure of nuclear donor parental protoplasts *Plant Sci.* **168** 303–8

- [23] Jo B H, Van Lerberghe L M, Motsegood K M and Beebe D J 2000 Three-dimensional micro-channel fabrication in polydimethylsiloxane (PDMS) elastomer *J. Microelectromech. Syst.* **9** 76–81
- [24] Baek J Y, Kwon G H, Kim J Y, Cho J H, Lee S H, Sun K and Lee S H 2007 Stable deposition and patterning of metal layers on the PDMS substrate and characterization for the development of the flexible and implantable micro electrode *Solid State Phenomena* **124** 165–8
- [25] Ju J I, Ko J-M, Kim S H, Baek J Y, Cha H-C and Lee S H 2006 Soft material-based microculture system having air permeable cover sheet for the protoplast culture of *Nicotiana tabacum* *Bioprocess Biosyst. Eng.* **29** 163–68
- [26] Jin J 2002 *The Finite Element Method in Electromagnetics* 2nd edn (New York: Wiley)
- [27] Nitsch J P and Nitsch C 1969 Haploid plants from pollen grains *Science* **163** 85–7
- [28] Stoicheva N and Dimitrov DS 1986 Frequency effects in protoplast dielectrophoresis *Electrophoresis* **7** 339–41
- [29] Puite K J, van Wikselaar P and Verhoeven H 1985 Electrofusion, a simple and reproducible technique in somatic hybridization of *Nicotiana plumbaginifolia* mutants *Plant Cell Rep.* **4** 274–6
- [30] Mehrle W, Naton M and Hampp R 1990 Determination of physical membrane properties of plant cell protoplasts via the electrofusion technique: prediction of optimal fusion yields and protoplast viability *Plant Cell Rep.* **8** 687–91
- [31] Neumann E, Gerisch G and Opatz K 1980 Cell fusion induced by high electric impulses applied to *Dictyostelium* *Naturwissenschaften* **67** 414–5